

1 Online Power and Efficiency Estimation of a Fuel Cell System for 2 Adaptive Energy Management Designs

3 Mohsen Kandidayeni^{a,b*}, Mehdi Soleymani^a, Alvaro Macias^c, João P. Trovão^{b,d}, Loïc Boulon^c

4 ^a Department of Mechanical Engineering, Faculty of Engineering, Arak University, Arak, 38156-8-8349, Iran

5 ^b e-TEESC lab, Department of Electrical and Computer Engineering, University of Sherbrooke, QC, J1K 2R1,
6 Canada

7 ^c Hydrogen Research Institute, Department of Electrical and Computer Engineering, Université du Québec à Trois-
8 Rivières, QC, G8Z 4M3, Canada

9 ^d Coimbra Institute of Engineering, Polytechnic of Coimbra, 3030-199, Coimbra, Portugal

10 _____

11 Abstract

12 The temporal changes of power and efficiency in a fuel cell (FC) stack can cause malperformance in the energy
13 management strategy (EMS) of a FC hybrid electric vehicle. Therefore, the online estimation of these physical
14 attributes is becoming an integral part of any EMS. This paper aims to utilize a two-step method to extract the
15 maximum power and efficiency points of a FC system online. In this respect, an online parameter estimation technique,
16 composed of smooth variable structure filter (SVSF) and Kalman filter (KF), is utilized in the first step to estimate the
17 parameters of a FC semi-empirical voltage model. KF generates statistically optimal estimates for a linear, well-
18 designed system model in the existence of Gaussian noise. However, these assumptions do not always hold in real
19 applications and can lead to unstable estimation. A practical solution to deal with these instabilities is to enforce
20 boundaries on the state estimates through SVSF which is based on sliding mode estimation concept. Hence, unlike the
21 other similar studies, this paper synthesizes the robustness of SVSF with the precision of KF to enhance the
22 characteristics estimation process of a FC stack. In the second step, the updated voltage model is utilized to extract
23 the efficiency and power curves of the real FC system. To corroborate the potential of the proposed approach, a

24 thorough comparison with KF, as an attested estimation method, is performed. The experimental tests on a 500-W FC
25 stack indicate the superior performance of the SVSF-KF compared to that of KF.

26 *Keywords:* Energy management strategy, Kalman filter, Parameter estimation, Proton exchange membrane fuel cell,
27 Smooth variable structure filter

28 **I. Introduction**

29 Electrification of vehicles is considered a promising solution for decreasing a considerable amount of greenhouse gas
30 emissions caused by transportation sector worldwide [1]. In this regard, several organizations are stressing the
31 potential role of hydrogen with the hope deploying fuel cell hybrid electric vehicles (FCHEVs) in different
32 transportation modes [2, 3]. The powertrain of a FCHEV is typically composed of a proton exchange membrane
33 (PEM) fuel cell (FC), as the primary power source, and a battery pack and/or a supercapacitor (SC) bank, as the
34 secondary one. Since these sources have different energetic characteristics in terms of power and efficiency, an energy
35 management strategy (EMS) is needed to distribute the power between them [4]. The main objective of an EMS is to
36 meet the requested power while minimizing the hydrogen consumption and maximizing the lifetime of power sources.
37 Several EMSs, rule-based, optimization-based, and intelligent-based, have been proposed for FCHEVs, as discussed
38 in [5]. Most of these strategies show very close performance to optimal results. However, the time-varying
39 characteristics of the FC system (power and efficiency) are not usually considered in these strategies. Hence, the
40 excellent results are merely valid for a short period of time [6, 7]. In [8], the importance of considering FC aging in
41 the design of an EMS based on deep reinforcement learning is discussed. In [9], the authors illustrate that the ignorance
42 of updating FC power and efficiency can increase the hydrogen consumption up to 6.6%. In this regard, some efforts
43 have been made to enhance the idea of health adaptation while developing an EMS. Some studies propose the
44 integration of a degradation model to develop a decision-making strategy based on prognostic of the power sources
45 [10, 11]. However, modeling the degradation mechanism under automotive conditions is still an open problem in the
46 literature. Some works suggest the use of an extremum seeking technique based on perturb and observe [12, 13].
47 Nevertheless, the simultaneous identification of several operating points, which is required in an EMS, highly
48 increases the complexity of these algorithms. The discussed shortfalls have led to the emergence of a new paradigm
49 for formulating an adaptive EMS based on online characteristics estimation in the FC system. Fig.1 illustrates the
50 main notion behind this concept. From this figure, an online estimation technique is used to update a FC model in the

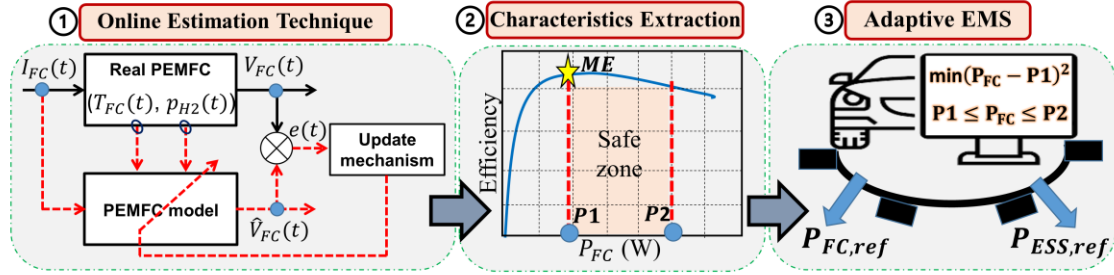


Fig. 1. The process of online characteristics estimation and its inclusion into an EMS design. (I_{FC} : FC current, T_{FC} : FC temperature, p_{H2} : hydrogen partial pressure, V_{FC} : FC measured voltage, \hat{V}_{FC} : FC estimated voltage, e : estimation error, ME : maximum efficiency point, P_{FC} : FC power, P_{ESS} : power of the energy storage system).

first step. Subsequently, the updated model is employed to extract the characteristic of the FC system. Finally, the obtained FC characteristics are utilized to define the boundaries and cost function of an EMS.

Several studies have been conducted on the online estimation of a FC model. In [14], a polynomial function is used to model the polarization behavior of a 1.3-kW PEMFC. The parameters of this model are estimated online by recursive least square (RLS). RLS is also employed to identify the parameters of a polynomial function representing the efficiency-vs.-power curve of a PEMFC stack in [15, 16] and hydrogen consumption-vs.-power of another stack in [17]. In [18], adaptive RLS is utilized to define a safe operating zone for the FC system of an electric tram. However, all the utilized FC models in [14-18] are purely empirical, derived by polynomial functions, without any insight into the underlying phenomena. These models lack generality and might not be able to simulate the complete FC behavior under different conditions. In [19], Ettahir et al. compare six semi-empirical FC models instead of using a polynomial function. They finally select a current-dependent model, suggested by Squadrito et al. [20], to estimate the polarization behavior of the FC. RLS and unscented Kalman filter (KF) are used to update the parameters of this model in [19, 21]. However, the performance of the utilized estimation techniques has not been compared. Moreover, the selected model does not take the stack temperature into consideration, which has a great impact on the FC performance. In this regard, in [22], the performance of RLS and KF estimation techniques are compared using Squadrito et al. and Amphlett et al. semi-empirical models. The latter is a multi-input model that considers current, temperature, and pressure to estimate the output voltage [23, 24]. This comparative study illustrates that the multi-input model (Amphlett) is more accurate than the single-input one (Squadrito), and KF is marginally more precise than RLS. The model proposed by Amphlett et al. has been validated for cold startup application in [25]. Moreover, it has become a benchmark model for testing the performance of metaheuristic optimization algorithms [26-28]. In [29], recursive maximum likelihood (RML) algorithm is compared with RLS to estimate the parameters of a PEMFC semi-empirical

77 model. This paper shows that RML and RLS lead to almost similar results when additional noise is not added to the
78 measured data. In [30], a data fusion method based on covariance intersection and KF is developed to extract the
79 polarization and power curves of a FC system using four semi-empirical models. The main problem with this method
80 is that the less accurate models can influence the estimation of the more accurate ones.

81 Considering the above-discussed estimation techniques, KF has been the most reliable regarding the parameters'
82 estimation of a FC model. However, certain complexities in the FC system modeling can violate the main assumptions
83 of this filter (linearity, Gaussian noise, etc.) and lead to instabilities in the estimation. Therefore, some papers have
84 also considered the stability and robustness aspects. In [31], an estimation technique based on Lyapunov is put forward
85 to identify two parameters of a nonlinear model composed of activation and ohmic overvoltages. In [32], an adaptation
86 law using the Lyapunov method is developed to update the parameters of a FC semi-empirical model for extracting
87 the power and voltage characteristics. The same estimation method is applied in [33] to a FC first-order equivalent
88 circuit model (ECM) to track the remaining useful life of the stack through identifying the internal resistance online.
89 However, the developed estimators based on Lyapunov in [31-33] are unique for the given problems and cannot be
90 generalized for other models and estimation techniques. A new recursive filter, known as smooth variable structure
91 filter (SVSF), is proposed in [34] to deal with the model uncertainties in a broader range. This filter is based on sliding
92 mode and variable structure concepts and compels the state estimates to change around their true values within a
93 boundary. SVSF has been successfully utilized in different engineering problems. Moreover, it has been shown that
94 this filter can be more stable and robust to model uncertainties compared to KF [35]. In [36], RLS is used to estimate
95 the parameters of a battery model, and SVSF is employed for estimating the battery state of charge (SOC). In [37],
96 SVSF is used for reliable SOC and state of health estimation of healthy and aged Lithium polymer cells. The performed
97 experiments indicate that SVSF can estimate the SOC more accurately than extended KF in uncertain scenarios caused
98 by aging or unknown initial values. However, SVSF is still a sub-optimal algorithm compared to KF since it is not
99 that robust to measurement noises. Therefore, researchers have suggested combining these methods (SVSF-KF) to
100 reach a trade-off between KF accuracy and SVSF robustness [38]. In [39], cubature KF and SVSF are combined to
101 improve the robustness and accuracy in the estimation of the effective bulk modulus in an electro-hydrostatic actuator.
102 In [40], KF and SVSF algorithms are merged to develop a thorough fault detection strategy for robust attitude
103 estimation in a small unmanned aerial vehicle (UAV) with faulty gyroscope signals. In [41], concurrent localization
104 and mapping is performed for an autonomous underwater vehicle utilizing a combined SVSF and extended KF.

105 This paper focuses on the first and second steps of the presented process in Fig. 1. In this regard, SVSF-KF
106 algorithm is proposed for the online power and efficiency characteristics estimation of a FC system. KF can result in
107 optimal estimation if all the underlying assumptions are respected. However, it is very sensitive to model uncertainties
108 which are ample in a FC system. SVSF is more stable and robust to model uncertainties but cannot handle a lot of
109 dynamics and measurement noise. Therefore, these two techniques can complement one another, considering the
110 robustness and accuracy. In particular, no study, to the best of the authors' knowledge, has considered the use of this
111 hybrid filter in the FC characteristics estimation. Since FC has a multivariate nature, its modeling certainly goes under
112 some uncertainties. In this regard, the semi-empirical model proposed by Amphlett et al. is used for modeling the
113 voltage behavior of a FC stack. The parameters of this model are estimated online by SVSF-KF, and the power and
114 efficiency characteristics curves are extracted from the updated model. Experiments are carried out on a 500-W
115 Horizon FC to verify the performance of the proposed method. Furthermore, a comparative study is performed with
116 KF as a well-known estimator in this line of work. The remainder of this paper is organized as follows. Section II
117 explains the utilized model for the PEMFC under study. The online estimation techniques are detailed in section III.
118 Section IV illustrates the experimental setup and analyzes the obtained results. Finally, the conclusion is given in
119 section V.

120 II. Fuel cell modeling

121 Fundamentally, the shape of voltage versus current curve is formed by three important irreversibilities in a PEMFC
122 [42]: 1) activation losses: the sluggishness of the reactions happening on the surface of the electrodes which have a
123 nonlinear effect on the voltage; 2) ohmic losses: direct resistance to the flow of electrons and ions through the
124 electrodes and the electrolyte which is linearly proportional the drawn current; 3) concentration losses: the alteration
125 in the concentration of the reactants at the electrodes' surface. The schematic polarization curve of a PEMFC,
126 including the three principal losses, is shown in Fig. 2. It should be noted that there is another voltage loss owing to
127 internal currents and fuel crossover in a FC system that is normally ignored while developing a semi-empirical model.
128 This loss is caused by a small amount of fuel passing across the electrolyte from the anode to the cathode and from
129 electron conduction along the electrolyte. The fuel loss and current are both small, and thus the net impact is normally
130 negligible [43].

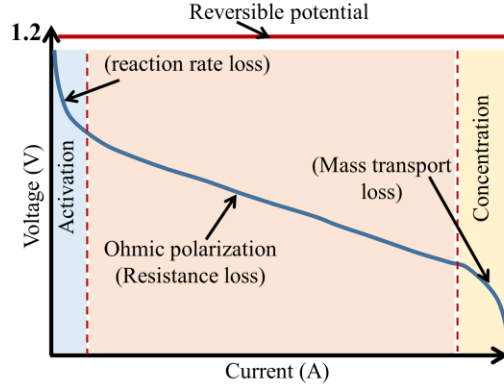


Fig. 2. Schematic polarization curve of a PEMFC cell.

131
132
133

134 The explained characteristics have led to the development of several semi-empirical models for describing the static
135 behavior of a PEMFC [20, 23, 24]. The general formulation of such models is expressed as:

$$136 \quad V_{FCN} = E_{Nernst} + V_{act} + V_{ohmic} + V_{con} \quad (1)$$

137 where V_{FCN} is the cell voltage, E_{Nernst} is the reversible cell potential, and V_{act} , V_{ohmic} , and V_{con} are the activation,
138 ohmic, and concentration losses, respectively. In this study, the model introduced by Amphlett et al. [23, 24] is utilized
139 to estimate the voltage of an open cathode PEMFC stack. As described earlier, this model has been fruitfully used for
140 modeling various PEMFC stacks [22, 44]. FC technology has been considerably improved since this model was
141 introduced. However, the structure of this model is still applicable, given that a suitable parameterization is required
142 to tune the parameters. Considering the number of cells (N_{cell}), the voltage of the PEMFC stack (V_{FC}) is given by:

$$143 \quad V_{FC} = N_{cell} V_{FCN} \quad (2)$$

144

145 E_{Nernst} is calculated by:

146

$$147 \quad E_{Nernst} = 1.229 - 0.85 \times 10^{-3}(T_{FC} - 298.15) + 4.3085 \times 10^{-5} T_{FC} [\ln(P_{H_2}) + 0.5 \ln(P_{O_2})] \quad (3)$$

148 where T_{FC} is the stack temperature (K), P_{H_2} is the hydrogen partial pressure in anode side ($N\ m^{-2}$), and P_{O_2} is the
149 oxygen partial pressure in the cathode side ($N\ m^{-2}$). V_{act} is determined by:

$$150 \quad \begin{cases} V_{act} = \xi_1 + \xi_2 T_{FC} + \xi_3 T_{FC} \ln(C_{O_2}) + \xi_4 T_{FC} \ln(I_{FC}) \\ C_{O_2} = \frac{P_{O_2}}{5.08 \times 10^6 \exp(-498/T_{FC})} \end{cases} \quad (4)$$

151 where $\xi_n (n = 1 \dots 4)$ are the semi-empirical coefficients based on fluid mechanics, thermodynamics, and
 152 electrochemistry, C_{O_2} is the oxygen concentration (mol cm^{-3}), and I_{FC} is the PEMFC operating current (A). V_{ohmic} is
 153 given by:

$$154 \quad V_{ohmic} = -I_{FC} R_{internal} = -I_{FC}(\zeta_1 + \zeta_2 T_{FC} + \zeta_3 I_{FC}) \quad (5)$$

155 where $R_{internal}$ is the internal resistor (Ω), and $\zeta_n (n = 1 \dots 3)$ are the parametric coefficients. Finally, V_{con} is
 156 calculated by:

$$157 \quad V_{con} = B \ln\left(1 - \frac{I_{FC}}{I_{max}}\right) \quad (6)$$

158 where B is a parametric coefficient (V), and I_{max} is the maximum current (A).

159 This paper aims to update the introduced voltage model online to extract the power and efficiency characteristics. In
 160 this regard, the model needs to be written as a linear-in-parameter equation in the sense of unknown parameters ($V_{FC} =$
 161 $\sum_{i=1}^{n_\theta} \theta_i x_i$, where θ_i is the unknown parameters of the model and x_i is the known values or regressors). Assuming
 162 $\theta^T = [\theta_1, \dots, \theta_{n_\theta}]$ and $X^T = [x_1, \dots, x_n]$ leads to $V_{FC} = X^T \theta$, where T is the transpose of a vector. In this work, V_{FC} ,
 163 T_{FC} , and I_{FC} are the three measurable states of the voltage model. To obtain the linear-in-parameter form of the voltage
 164 model, using (1) to (6) results in:

$$165 \quad V_{FC} - E_{nernst} = X^T \theta \quad (7)$$

166 where

$$\theta^T = [\xi_1, \xi_2, \xi_3, \xi_4, \zeta_1, \zeta_2, \zeta_3, B]$$

$$X^T = [1, T_{FC}, T_{FC} \ln(C_{O_2}), T_{FC} \ln(I_{FC}), -I_{FC}, -I_{FC} T_{FC}, -I_{FC}^2]$$

167 The power of the FC system (P_{FCS}) is calculated by subtracting the FC stack power (P_{FC}) from the consumed power
 168 by the auxiliary systems (P_{Aux}):

$$169 \quad P_{FCS} = P_{FC} - P_{Aux} \quad (8)$$

$$170 \quad P_{FC} = V_{FC} \times I_{FC} \quad (9)$$

$$171 \quad P_{Aux} = P_{fan} + P_{valve} \quad (10)$$

$$172 \quad P_{fan} = c_1 D_{fan}^2 + c_2 D_{fan} + c_3 \quad (11)$$

173 $P_{Valve} = V_{Valve} \times I_{Valve}$ (12)

174 where P_{fan} is the power consumption of the cooling fan, c_1, c_2, c_3 are empirical parameters, D_{fan} is the duty cycle of
 175 the fan, P_{Valve} denotes the consumed power by the hydrogen valve, and V_{Valve} and I_{Valve} are the voltage and current
 176 of the hydrogen valve respectively. The empirical parameters and the power consumption of the hydrogen valve are
 177 obtained by experiments on the real system. The purge valve power consumption is ignored due to having a fixed
 178 cyclic purging (every 10 s for a duration of 100 ms). Finally, the efficiency of the FC system (η_{FCS}) can be calculated
 179 based on its voltage [45], as:

180
$$\begin{cases} \eta_{FCS} = \frac{P_{FCS}}{P_{H2}} = \frac{V_{FCS} \times I_{FC}}{\Delta H \times \frac{I_{FC}}{nF}} = \frac{V_{FCS}}{1.254} \\ V_{FCS} = \frac{P_{FC} - P_{Aux}}{I_{FC}} = V_{FC} - \frac{P_{Aux}}{I_{FC}} \end{cases}$$
 (13)

181 where P_{H2} is the energy value of consumed hydrogen (W), V_{FCS} is the voltage of the FC system, ΔH is the hydrogen
 182 higher/lower heating value (kJ/mol), n is the number of electrons transferred for each molecule of fuel (which is 2
 183 for hydrogen-oxygen reaction), and F is the Faraday constant. Considering the hydrogen lower heating value ($\Delta H =$
 184 241 kJ/mol) in $\frac{\Delta H}{nF}$, 1.254 is achieved as the so-called thermoneutral potential.

185

186 III. Online parameter estimation algorithms

187 The areas of parameter and state estimation are highly important for the further development of PEMFC technology.
 188 As discussed in the introduction section, several methods, such as RLS, KF, and Lyapunov-based estimation, have
 189 been used for parameters estimation of PEMFC semi-empirical models. RLS minimizes a weighted linear least-
 190 squares cost function by recursively determining the coefficients that are related to the deterministic input signals.
 191 Therefore, the estimated state is solely updated by the available measurements. KF can update and estimate an
 192 evolving state since it has two stages of operation: prediction and correction. In the prediction stage, a model of the
 193 system is used to predict the evolution of the states even in the absence of measurement. In the correction stage, the
 194 difference between the current prediction and the current observation is employed to refine the state estimate. As
 195 reported in [22], KF can yield marginally better estimates in a FC system compared to RLS. However, both techniques
 196 might result in unstable estimates while working in a real FC system. This is due to the fact that their assumptions,
 197 Gaussianity of process and measurement covariances, could be violated. Therefore, the robustness aspect of the

198 algorithm should be considered as well as the accuracy. In this regard, Lyapunov-based estimation has been suggested
199 which can guarantee stability in a particular system. That means by changing the FC model, the Lyapunov function
200 needs to be updated. However, it is not always easy to find a new function for this purpose. The above-discussed
201 aspects have turned the attention of this manuscript to the employment of SVSF which has been introduced as a robust
202 estimator in the literature. SVSF has an integral switching action to assure the convergence of estimation within the
203 vicinity of real values. The key performance benefits of the SVSF over the discussed estimation methods are as
204 follows:

- 205 • The discussed filtering methods are developed based on the precise knowledge of the system's model.
206 Nevertheless, substantial noise and uncertainties can arise in a real application. For instance, when the FC
207 system experiences degradation, fault conditions, or any performance drifts, the developed model is not
208 precise anymore, and this may afflict the performance of the discussed estimators. On the other hand, SVSF
209 maintains robustness and stability within a preset range for bounded uncertainties and noise levels. Hence,
210 SVSF is not reliant on a precise model under uncertain conditions.
- 211 • The discussed techniques provide the error between measurement and estimation as a performance index.
212 Besides this, SVSF provides an index using the chattering signal [34], which can be related to the state of
213 health of the system. This feature is useful in health monitoring studies.
- 214 • The nonlinear versions of the discussed estimators normally require local linearization of the nonlinear
215 function around a fixed point to estimate the nonlinear states of the model. This could diminish the optimality
216 and precision of the filter. However, SVSF carries out this nonlinear state estimation without any
217 approximation. It should be noted that for systems with nonlinear measurement models, SVSF also requires
218 local linearization, similar to other filters.

219 With all the favorable attributes of SVSF algorithm, it is still considered a suboptimal estimator. It is thus advantageous
220 to combine the robust performance of SVSF with accurate performance of KF, as suggested in [38-41].

221 Generally, a linear dynamic system and a measurement model are characterized by:

$$222 \quad x_{k+1} = Ax_k + Bu_k + w_k \tag{14}$$

$$223 \quad z_{k+1} = Hx_{k+1} + v_{k+1} \tag{15}$$

224 where x is the state vector, k is the time index, A is the linear system transition matrix, B is the input gain matrix, u
 225 is the input vector, w is the system noise vector, z is the measurement vector (system output), H is the linear
 226 measurement matrix, and v is the measurement noise vector. In what follows, KF and the hybrid SVSF-KF methods
 227 are explained for the parameter estimation of the model introduced in (14) and (15).

228 **A. Kalman filter**

229 KF is one of the most practiced filters for linear dynamic systems. It offers an optimal solution in the presence of
 230 Gaussian white noise if all the fundamental assumptions hold [46]. It employs measurements that are linearly linked
 231 to the system's states/parameters and error covariance matrices to calculate the Kalman gain. This gain is applied to
 232 the a priori state estimate to generate an updated estimate of the states. This predictor-corrector estimation process is
 233 continued in an iterative manner. In this regard, a priori estimate based on the system definition is given by:

$$234 \hat{x}_{k+1|k} = \hat{A}\hat{x}_{k|k} + \hat{B}u_k \quad (16)$$

235 where $\hat{\cdot}$ denotes the estimated vector or values. The corresponding state error covariance matrix (P) is defined by:

$$236 P_{k+1|k} = HP_{k|k}H^T + Q_k \quad (17)$$

237 where Q is the noise covariance matrix of the system, and T is the transpose of some vector or matrix. The Kalman
 238 gain (K) is determined by:

$$239 K_{k+1} = P_{k+1|k}H^T[HP_{k+1|k}H^T + R_{k+1}]^{-1} \quad (18)$$

240 where R is the measurement noise covariance matrix. Using the calculated Kalman gain, the state estimate is updated
 241 as:

$$242 \hat{x}_{k+1|k+1} = \hat{x}_{k+1|k} + K_{k+1}[z_{k+1} - H\hat{x}_{k+1|k}] \quad (19)$$

243 Finally, a posteriori state error covariance matrix is determined by:

$$244 P_{k+1|k+1} = [I - K_{k+1}H]P_{k+1|k} \quad (20)$$

245 where I is an identity matrix.

246 **B. Combined smooth variable structure and Kalman filter**

247 KF is developed based on the accurate knowledge of the system model and assumes measurement noises are white.
 248 However, these assumptions do not always hold under real applications, especially when the system confronts aging,
 249 fault conditions, or any other abnormalities. The violation of the assumptions can degrade the performance of KF
 250 since the system model is not accurate anymore. SVSF is a fairly new predictor-corrector estimation method that
 251 generates suboptimal but highly robust and stable estimates against modeling uncertainties and errors. The preserved
 252 robustness and stability of SVSF are due to enforcing the state estimates to change within a boundary layer around the
 253 true state trajectory. However, compared to KF, SVSF is still a sub-optimal filter which implies that there is a trade-
 254 off between robustness to modeling uncertainties and estimation precision. In this regard, a combination method has
 255 been proposed based on the definition of a time-varying boundary layer in [47] to preserve the SVSF robustness while
 256 profiting from the exactness of KF. This method provides the basis for the combination of SVSF with extensions of
 257 KF and even other existing estimation techniques. The SVSF-KF iterative estimation process is summarized in (21)
 258 to (31). Similar to KF, the prediction step begins with the calculation of $\hat{x}_{k+1|k}$ and $P_{k+1|k}$ as follows.

$$259 \quad \hat{x}_{k+1|k} = \hat{A}\hat{x}_{k|k} + \hat{B}u_k \quad (21)$$

$$260 \quad P_{k+1|k} = HP_{k|k}H^T + Q_k \quad (22)$$

261 Subsequently, a priori measurement error ($e_{z,k+1|k}$) and the measurement error covariance matrix (S_{k+1}) are
 262 calculated as:

$$263 \quad e_{z,k+1|k} = z_{k+1} - H\hat{x}_{k+1|k} \quad (23)$$

$$264 \quad S_{k+1} = H_{k+1}P_{k+1|k}H_{k+1}^T + R_{k+1} \quad (24)$$

265 At this point, a time-varying smoothing boundary layer ($\psi_{VBL\ k+1}$) is calculated and utilized to combine SVSF and
 266 KF:

$$267 \quad \psi_{VBL\ k+1} = (\bar{A}^{-1}HP_{k+1|k}H^TS_{k+1}^{-1})^{-1} \quad (25)$$

268 where the bar notation signifies a diagonal matrix ($\bar{A} = \text{diag}(A)$), and A is obtained by:

$$269 \quad A = (|e_{z,k+1|k}| + \gamma|e_{z,k|k}|) \quad (26)$$

270 where γ is the convergence rate ($0 < \gamma < 1$). By comparing the defined $\psi_{VBL\ k+1}$ with a constant smoothing boundary
 271 layer ($\psi_{Con.}$), proposed by the designer, the update gain is defined as follows:

$$272 \begin{cases} \text{If } \psi_{VBL\ k+1} \geq \psi_{Con.}: K_{k+1} = H^+ \text{diag}[A \circ \text{sat}(\bar{\psi}_{Con.}^{-1}, e_{z,k+1|k})](\overline{e_{z,k+1|k}})^{-1} \\ \text{If } \psi_{VBL\ k+1} < \psi_{Con.}: \text{Use Kalman gain defined in (18)} \end{cases} \quad (27)$$

273 where H^+ is the Pseudoinverse of H , \circ denotes element-by-element multiplication, and the saturation function is
 274 calculated as:

$$275 \text{sat}(\bar{\psi}_{Con.}^{-1}, e_{z,k+1|k}) = \begin{cases} 1, & e_{z,k+1|k}/\bar{\psi}_{Cons.} \geq 1 \\ e_{z,k+1|k}/\bar{\psi}_{Cons.}, & -1 < e_{z,k+1|k}/\bar{\psi}_{Cons.} < 1 \\ -1, & e_{z,k+1|k}/\bar{\psi}_{Cons.} \leq -1 \end{cases} \quad (28)$$

276 In fact, when the value of $\psi_{Con.}$ in the standard SVSF gain is larger than the $\psi_{VBL\ k+1}$, estimation accuracy is decreased
 277 owing to the difference between the constant layer and the upper layer. In this case, Kalman gain should be applied to
 278 achieve a more precise result. However, when the $\psi_{VBL\ k+1}$ goes beyond the $\psi_{Con.}$, it indicates the existence of
 279 modeling uncertainty (which can result in a loss in estimation accuracy). In this case, the SVSF gain in (27) should be
 280 employed to assure a stable estimate. After choosing the update gain, the updated state estimates ($\hat{x}_{k+1|k+1}$), state error
 281 covariance matrix ($P_{k+1|k+1}$), and the a posteriori measurement error ($e_{z,k+1|k+1}$) are defined by:

$$282 \hat{x}_{k+1|k+1} = \hat{x}_{k+1|k} + K_{k+1}e_{z,k+1|k} \quad (29)$$

$$283 P_{k+1|k+1} = (I - K_{k+1}H)P_{k+1|k}(I - K_{k+1}H)^T + K_{k+1}R_{k+1}K_{k+1}^T \quad (30)$$

$$284 e_{z,k+1|k+1} = z_{k+1} - H\hat{x}_{k+1|k+1} \quad (31)$$

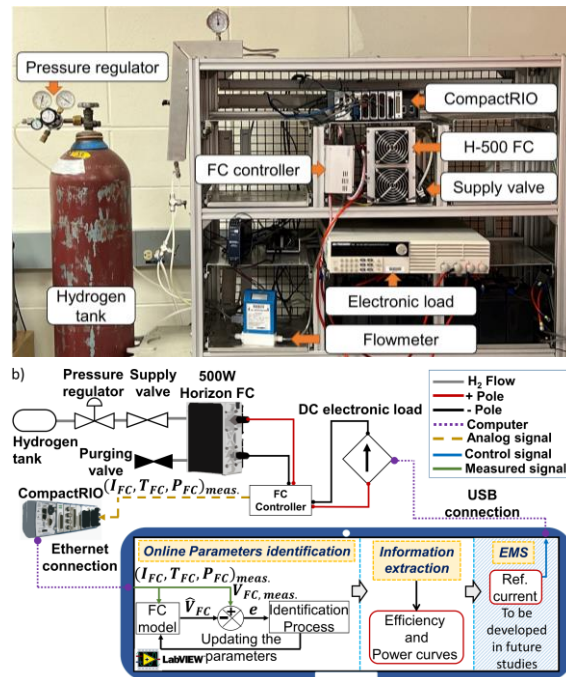
285 IV. Experiments and results analysis

286 An experimental test bench has been developed to corroborate the performance of the explained online estimation
 287 methods. Hereunder, the utilized setup is explained first. Subsequently, the considered scenarios and the achieved
 288 outcomes concerning the characteristics estimation are completely discussed.

289 A. Experimental setup

290 Fig. 3 demonstrates the developed setup for the purpose of this work. As is seen, a Horizon H-500 FC is utilized to
 291 collect the required data for the estimation process. It is an air-cooled FC equipped with two axial fans to provide

292 oxygen on the cathode side and control the stack temperature. This FC is self-humidified and works based on a dead-
 293 ended anode (DEA) principle. In this regard, the dry hydrogen is continuously supplied by a hydrogen supply valve
 294 in the anode inlet at a predefined pressure. The flow rate of hydrogen is between 0 and 6.5 l/min , depending on the
 295 requested current from the stack. The voltage of the hydrogen valve (V_{valve}) is 12 V, and the current of the hydrogen
 296 valve (I_{valve}) is 0.72 A. A manual forward pressure regulator is employed to maintain the partial pressure of hydrogen
 297 between 0.45 and 0.55 bar. A DEA system simplifies the FC balance of plant as a hydrogen recirculation loop (pump,
 298 water separator, and humidifier) will not be needed. Furthermore, during the DEA operation, water backflow in the
 299 anode around the membrane relatively leads to self-humidification. The anode outlet has a hydrogen purging valve to
 300 remove the accumulated water in the catalyst and gas diffusion layers of anode. It also pushes out the nitrogen
 301 dispersed from the cathode across the membrane. This valve is normally closed and conducts a cyclic purging (every
 302 10 s for a duration of 100 ms) while the FC is under operation. An OMEGA flowmeter (FMA-A2309), calibrated for
 303 hydrogen gas, is employed to measure the hydrogen flow. This flowmeter does not require any temperature, pressure,
 304 or square root corrections since it has a capillary thermal technology to determine mass flow accurately. Table I
 305 provides the specifications of the explained FC system.



306
 307 Fig. 3. The experimental setup for testing the online estimation methods, a) testbench picture, b) connection diagram and flow chart code.
 308
 309

310
311

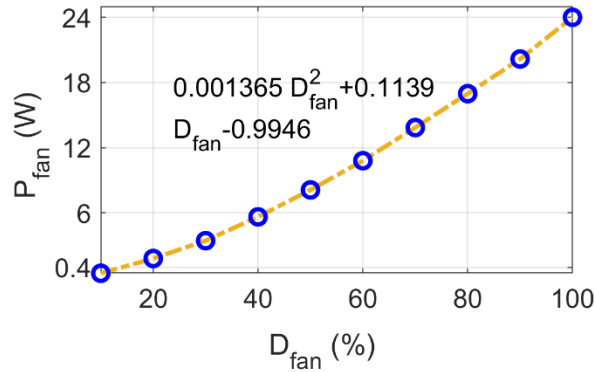
TABLE I
SPECIFICATIONS OF THE HORIZON H-500 PEMFC

PEMFC technical data	
Type	Open cathode
Number of cells	24
Hydrogen pressure	0.45-0.55 bar
Cathode pressure	1 bar
Ambient temperature	5 °C to 30 °C
Maximum stack temperature	65 °C
Over current shut down	42 A
Hydrogen purity	≥ 99.995% dry H ₂
Size	130 mm × 268 mm × 122.5 mm
Cooling	Air (integrated cooling fan)

312

313 As demonstrated in Fig. 3b, a National Instrument CompactRIO (NI cRIO-9022) is connected to the FC controller to
314 measure the current, temperature, and voltage signals for the estimation purposes. The cRIO communicates with the
315 PC via an Ethernet connection. LabVIEW software is accessible in the PC. The data transfer between the cRIO and
316 the PC is done with a 10-Hz frequency. An 8514 BK Precision DC Electronic Load is used to draw a load profile from
317 the FC system. Fig. 4 shows the power consumption curve of the cooling fan obtained by measuring its voltage and
318 current in different duty cycles. The fitting parameters in (11) have been extracted from Fig. 4. It should be noted that
319 all the tests in this work have been done under the constant cooling fan duty cycle of 34%. If the FC stack temperature
320 reaches 60°C, the duty cycle will change to 100% to avoid over temperature shut down.

321



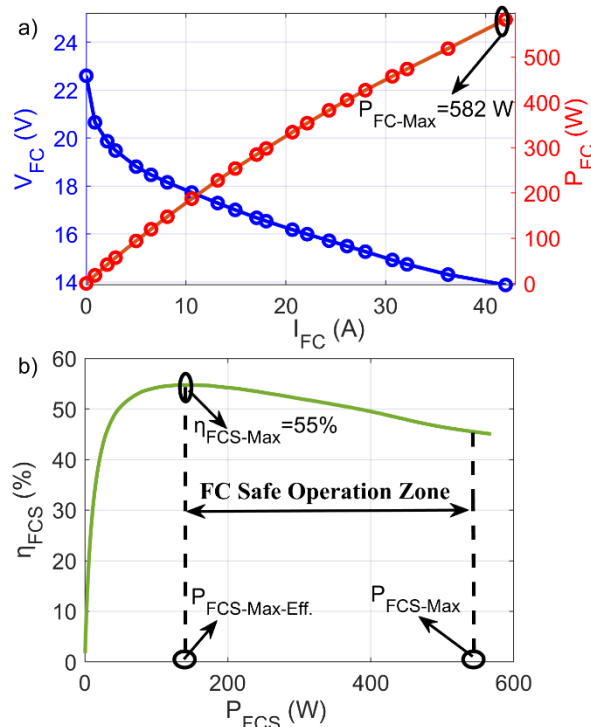
322

323 Fig. 4. Consumed power by the cooling fan with respect to duty cycle.

324

325 The actual health state of the explained FC installed on the setup is unknown as it has been used in diverse projects.
326 Hence, to illuminate its actual operational characteristics, the experimental polarization, power, and efficiency curves
327 of this FC are shown in Fig. 5. These characteristics will be employed as the reference curves to assess the performance
328 of the developed adaptive estimator. The measured voltage/power points have been obtained by drawing constant

329 current from the FC system in different levels. It should be noted that the characteristics curves have been extracted
 330 at ambient temperature of 15°C with the humidity level of 60%. According to Fig. 5a, the utilized FC can reach a
 331 maximum power of 582 W at 42 A. The maximum recommended current to be drawn from this FC is 42 A, and the
 332 low voltage shut down is 12 V. The efficiency curve of the FC system in the mentioned ambient conditions is presented
 333 in Fig. 5b. From this figure, this FC has gained a maximum efficiency of 55% at around 143 W considering the
 334 hydrogen lower heating value. The efficiency curve has been obtained using (13) and considering the auxiliary system
 335 power loss explained in (8) to (12). It should be borne in mind that the relation between efficiency and voltage in a
 336 PEMFC depends on whether the system or the stack is considered. From Fig. 5, initially, the FC stack voltage has the
 337 maximum value while the corresponding efficiency of the FC system is zero. However, the relation between the
 338 voltage of the FC system (V_{FC}) and the efficiency of the FC system (η_{FCS}) is direct, as shown in (13). Fig. 5b also
 339 demonstrates a defined safe operation zone for a FC system which is located between the power corresponding to the
 340 maximum efficiency ($P_{FCS-Max-Eff.}$) and the maximum power of the FC system ($P_{FCS-Max}$). This zone has been
 341 utilized in several studies for designing an EMS [14, 15, 48, 49]. In fact, operation within this zone leads to the increase

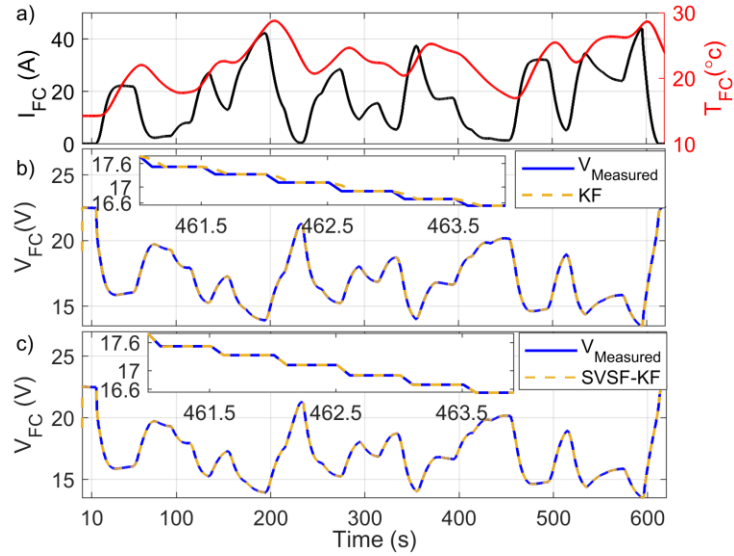


342
 343 Fig. 5. The reference characteristics of the used PEMFC; a) polarization and power curves obtained by measured data ($P_{FCS-Max}$: maximum
 344 power of the FC system), and b) efficiency curve calculated by measured voltage ($\eta_{FCS-Max}$: maximum efficiency of the FC system) along with
 345 the representation of the FC safe operation zone.
 346

347 of the FC lifetime and fuel economy. This is mainly due to the fact that by sticking to this zone, FC system is prevented
 348 from working in open circuit voltage and low-power regions. Moreover, high-power operation zone is only used when
 349 the EMS needs to meet very high-power demand. Therefore, the FC system will operate around its maximum
 350 efficiency point most of the time.

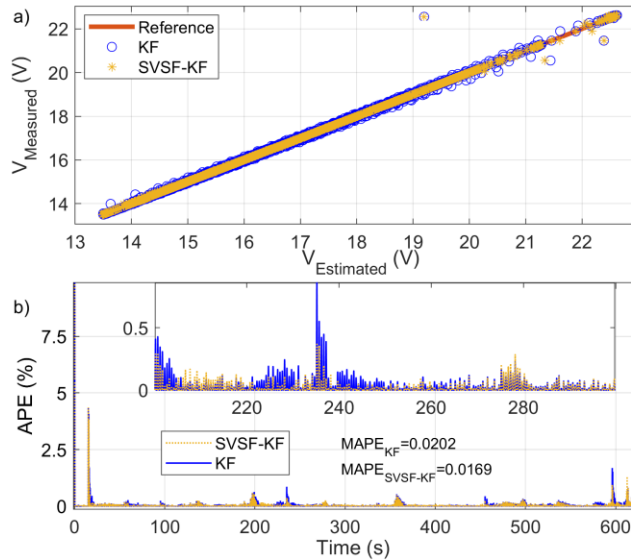
351 **B. Results and discussion**

352 A dynamic current profile, as shown in Fig. 6a, is applied to the FC stack to evaluate the performance of the proposed
 353 combined SVSF-KF for online characteristics estimation of the Horizon FC. This dynamic profile along with its
 354 corresponded voltage and temperature are recorded for comparison purposes. As is seen, the current profile is 620 s,
 355 which leads to 6200 measured data points by having a frequency of 10 Hz for performing the measurement. This
 356 dynamic profile covers the minimum and maximum operating current of the FC stack and can provide a good
 357 excitation to the system for conducting the online estimation. Fig. 6b represents the estimation of FC stack voltage by
 358 KF, and Fig. 6c illustrates the same estimation by the proposed SVSF-KF. From these figures, both adaptive filters
 359 are able to estimate the stack voltage with very high accuracy. Fig. 7 compares the estimated output voltage by SVSF-
 360 KF and KF. Fig. 7a demonstrates the parity plot of the estimated stack voltage by each of the techniques. From this
 361 figure, a high density of the estimated voltage points by both techniques is placed on the reference line and dispersed
 362 very close to it. This parity plot justifies the satisfactory performance of the proposed hybrid method (SVSF-KF) in
 363 terms of voltage estimation as it has reached similar and, on some occasions, better results than KF. Fig. 7b also
 364 indicates the absolute percentage error (APE: $\left| \frac{V_{measured} - V_{estimated}}{V_{measured}} \right| \times 100$) and the mean absolute percentage error
 365 (MAPE: $\frac{100}{n} \sum_{i=1}^n \left| \frac{V_{measured}^{(i)} - V_{estimated}^{(i)}}{V_{measured}^{(i)}} \right|$) for each of the methods. According to this figure, SVSF-KF has achieved
 366 the MAPE of 0.0169 while KF has reached the MAPE of 0.0202. It is worth noting that the estimation mismatch
 367 around 22 V of measured voltage in Fig. 7a, which corresponds to the jump in the beginning of voltage estimation in
 368 Fig. 7b, is due to the initialization of the unknown parameters. This behavior swiftly disappears after the convergence
 369 of the algorithms. Since both estimation techniques have been tested with the same initial unknown model parameters,
 370 they have experienced the same jump in the beginning of estimation process. Overall, it can be said from Fig. 7 that
 371 both estimation methods have a very good level of precision for estimating the voltage. In fact, this is due to the fact
 372 that at each point, they just try to minimize the error between estimated and measured voltage.



373
374
375
376
377

Fig. 6. Online voltage estimation by the utilized adaptive filters; a) applied current the FC stack (solid line in black) and the corresponding measured stack temperature (solid line in red), b) comparison of measured voltage with the estimated one by KF, c) comparison of measured voltage with the estimated one by SVSF-KF.

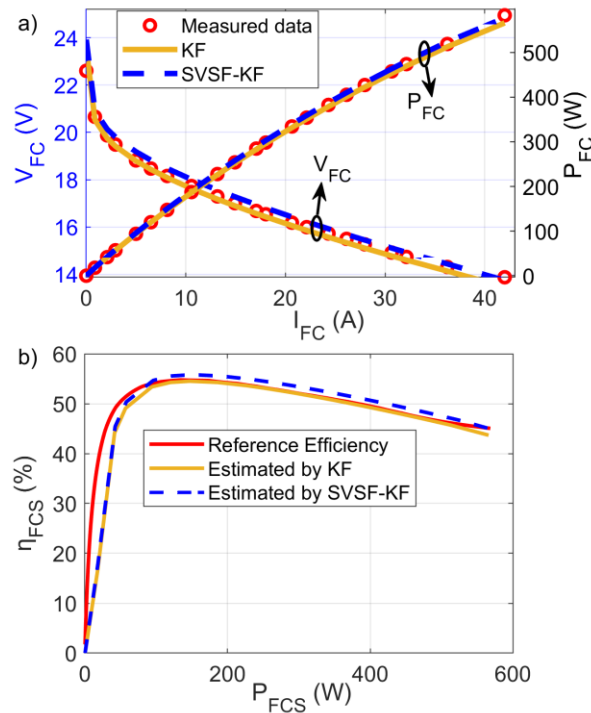


378
379
380
381

Fig. 7. Comparison of the voltage estimation by the deployed methods; a) Parity plot of voltage estimation by both techniques, b) the achieved absolute percentage error (APE) and mean absolute percentage error (MAPE) of estimated voltage by KF and SVSF-KF.

382 However, for the purpose of this work, it is highly important to check whether the updated semi-empirical voltage
383 model is able to accurately estimate the power and efficiency characteristics in the whole operating range of the FC
384 stack. In fact, maximum power is normally among the considered constraints of the system and maximum efficient
385 power is used in the formulation of the cost function in an energy management application. The EMS can be prevented
386 from malfunction by updating the values of maximum power and efficiency. To this end, the updated model by the
387 estimation methods have been used to generate the power and estimation curves. Fig. 8 presents the extracted

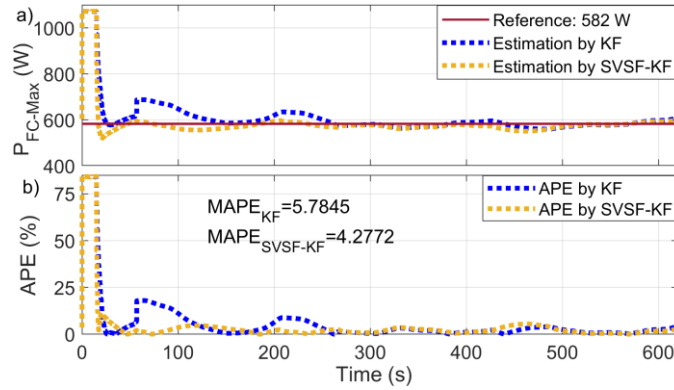
388 characteristics from the updated model. From this figure, it is observed that the updated model by both adaptive filters
 389 is capable of estimating precise polarization, power, and efficiency curves. These curves have been extracted by using
 390 the obtained parameters at 280 s. To obtain the maximum power and efficiency points at each moment, these two
 391 curves need to be plotted at each instant. Then, the maximum value can be easily detected at each curve. Regarding
 392 the precision of the estimated characteristics in Fig. 8, no specific conclusion can be still made. Since these curves
 393 belong to just one moment, they can change in the next or the previous moment. Therefore, the estimation of maximum
 394 power and efficiency points at each instant should come under scrutiny.



395 Fig. 8. The estimated characteristics of the PEMFC stack at 280 s; a) polarization and power curves, and b) efficiency curve.
 396
 397
 398

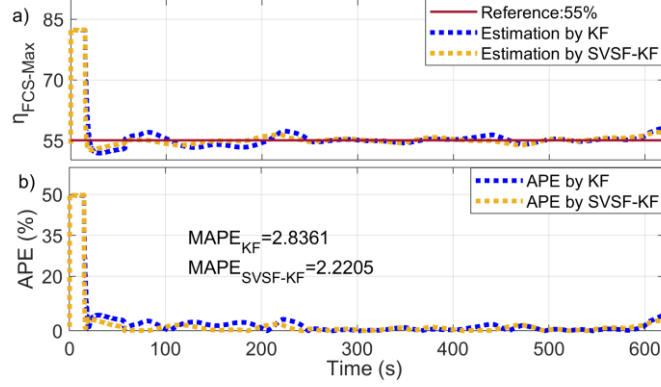
399 Fig. 9a and Fig. 9b represent the maximum power point tracking and the estimation error by both methods. To obtain
 400 Fig. 9a, the estimated power curve of the FC model has been plotted at each timestep, and the maximum value has
 401 then been extracted from it. This figure illustrates the required time to obtain the targeted characteristics from the
 402 model. The considered reference maximum power is 582 W according to the illustrated experimental power curve in
 403 Fig. 5a. Since the performed test is not very long, this value is not expected to change due to degradation. According
 404 to Fig. 9a, there is a big jump in the beginning of maximum power point estimation leading to considerable error.
 405 SVSF-KF almost converges after around 80 s while KF keeps the jumpy behavior up to around 250 s. From this point

406 (250 s) on, both methods almost show similar behavior. This behavior explains the reason for similarity of the
 407 extracted characteristics at 280 s in Fig. 8. From Fig. 9b, the achieved MAPE by SVSF-KF is almost 1.5 % less than
 408 that of KF. It is worth reminding that the APE and MAPE of KF and SVSF-KF have been calculated with respect to
 409 their performance compared to reference maximum power (582 W).



410
 411 Fig. 9. Maximum power point tracking during the whole profile; a) estimation of maximum power point at each moment, and b) maximum
 412 power point estimation error considering $P_{FC-Max} = 582 W$ as the reference point.

413 Fig. 10a illustrates the estimation of the maximum efficiency point. Moreover, the estimation error is shown in Fig.
 414 10b. During this estimation process, the error has been calculated with regard to the reference maximum efficiency
 415 (55%). From this figure, it is also observed that there is a big error in the beginning of the estimation process and after
 416 that the error decreases to less than three percent for both methods. Overall, the achieved MAPE by SVSF-KF is
 417 almost 0.6 % less than the one obtained by KF. From Fig. 9 and Fig. 10, it can be stated that the estimation of maximum
 418 power is more challenging than maximum efficiency. This is due to the fact that the changes in the FC power are
 419 much sharper than the efficiency. It should be noted that the big jump in the beginning of voltage, maximum efficiency,
 420 and maximum power estimations is due to the initialization of unknown model parameters, which is the same in both
 421 algorithms. Another worth noting aspect is that if the performance of the algorithms is compared from 250 s to 600 s
 422 (that means after the convergence of KF), it is realized that both techniques lead to almost similar results (Maximum
 423 power estimation: $MAPE_{KF}: 2.09$, $MAPE_{SVSF-KF}: 2$, Maximum efficiency estimation: $MAPE_{KF}: 1.01$,
 424 $MAPE_{SVSF-KF}: 1$). Assuming a perfectly known model, both algorithms will reach nearly the same results even in a
 425 longer test as SVSF-KF uses the same gain as KF to update the estimates in normal conditions. In uncertain conditions,
 426 it uses its own particular gain which is more robust than Kalman gain. In fact, this is the principal reason for combining
 427 these filters.



428

429 Fig. 10. Maximum efficiency point tracking during the whole profile; a) estimation of maximum efficiency point at each moment, and b)
 430 maximum efficiency point estimation error considering $\eta_{FC-Max} = 55\%$ as the reference point.

431 **V. Conclusion**

432 Since a FC stack has time-varying maximum power and efficiency points, their online estimate is vital in energy
 433 management of FCHEVs. KF is known as an optimal estimator if all the necessary assumptions, like normal
 434 distribution of all uncertainties, hold. However, these assumptions can be easily violated in a FC stack that is a multi-
 435 physical system. One of the well-established solutions to enhance the estimation robustness in this case is to impose
 436 limits on the targeted parameters. This can be conveniently accomplished by using SVSF that is based on principle of
 437 sliding mode estimation. Thus, this paper puts forward a new estimation method composed of SVSF and KF to
 438 estimate the characteristics of a FC stack online. To this end, a semi-empirical FC model, proposed by Amphlett et
 439 al., is utilized to determine the output voltage of a 500-W FC stack. The parameters of the utilized model are tuned
 440 online by the combined SVSF-KF algorithm. Then, the updated model is employed to extract the power and efficiency
 441 curves of the stack at each moment. The performance of this method is compared with KF, which is an attested method
 442 in the literature. The obtained experimental results, using a developed test bench with a 500-W open cathode Horizon
 443 FC stack, indicate that the combined SVSF-KF has superior performance compared to KF in terms of accuracy in
 444 voltage, maximum power, and maximum efficiency estimation. Regarding the voltage estimation, the MAPE has
 445 decreased from 0.0202 (attained by KF) to 0.0169 (attained by SVSF-KF), marking 16.3 % of error reduction. In case
 446 of power and efficiency, the MAPE values have declined from 5.7845 and 2.8361 (obtained by KF) to 4.2772 and
 447 2.2205 (obtained by SVSF-KF) respectively, indicating 26 % and 21.7 % of improvement in the estimation accuracy.
 448 The presented work in this manuscript provides the basis for designing an adaptive EMS for a FCHEV. In future, the
 449 proposed combined filter should be combined with an EMS to estimate the FC characteristics in real-time. This
 450 integration enhances the efficiency and robustness of the EMS when the FC characteristics go under temporal changes.

451 **Declaration of competing interest**

452 The authors declare that they have no known competing financial interests or personal relationships that
453 could have appeared to influence the work reported in this paper.

454 **Acknowledgments**

455 This work was supported in part by the Fonds de Recherche du Québec Nature et Technologies (FRQNT) (284914 &
456 283370), Réseau Québécois sur l’Energie Intelligente (postdoctoral and third cycle scholarships), Natural Sciences
457 and Engineering Research Council of Canada (NSERC) [RGPIN-2018-06527 and RGPIN-2017-05924], and Canada
458 Research Chairs program [950-230863 and 950-230672].

459 **Nomenclature**

460	APE	Absolute percentage error
461	cRIO	CompactRIO
462	DEA	Dead-ended anode
463	ECM	Equivalent circuit model
464	EMS	Energy management strategy
465	FC	Fuel cell
466	FCHEV	Fuel cell hybrid electric vehicles
467	KF	Kalman filter
468	MAPE	Mean absolute percentage error
469	NI	National Instrument
470	PEM	Proton exchange membrane
471	QP	Quadratic programming
472	RLS	Recursive least square
473	RML	Recursive maximum likelihood
474	SC	Supercapacitor
475	SOC	State of charge
476	SVSF	Smooth variable structure filter
477	SVSF-KF	Combined smooth variable structure and Kalman filters

478 UAV Unmanned aerial vehicle

479 **Symbols**

480 T Transpose of a vector

481 \bar{A} Diagonal matrix of A

482 C_{O_2} Oxygen concentration (mol cm^{-3})

483 D_{fan} Duty cycle of the fan (%)

484 E_{Nernst} Reversible cell potential (V)

485 H^+ Pseudoinverse of H

486 I_{FC} PEMFC operating current (A)

487 I_{valve} Hydrogen valve current (A)

488 I_{max} Maximum current (A)

489 N_{cell} Number of cells

490 P_{Aux} Consumed power by the auxiliary systems (W)

491 P_{FC} FC stack power (W)

492 P_{FCS} Power of the FC system (W)

493 $P_{FCS-Max}$ Maximum power of the FC system

494 P_{H_2} Energy value of consumed hydrogen (W)

495 P_{H_2} Hydrogen partial pressure in anode side (N m^{-2})

496 P_{O_2} Oxygen partial pressure in the cathode side (N m^{-2})

497 P_{valve} Consumed power by hydrogen valve (W)

498 P_{fan} Power consumption of the cooling fan (W)

499 $R_{internal}$ Internal resistor (Ω)

500 S_{k+1} Measurement error covariance matrix

501 T_{FC} Stack temperature (K)

502 V_{FC} Voltage of the PEMFC stack (V)

503 V_{FCN} Cell voltage (V)

504 V_{valve} Hydrogen valve voltage (V)

505	V_{act}	Activation loss (V)
506	V_{con}	Concentration loss (V)
507	V_{ohmic}	Ohmic loss (V)
508	c_1, c_2, c_3	Empirical parameters
509	$e_{z,k+1 k}$	A priori measurement error
510	x_i	Known values or regressors
511	ζ_n	Parametric coefficients
512	$\eta_{FCS-Max}$	Maximum efficiency of the FC system
513	θ_i	Unknown parameters
514	ξ_n	Semi-empirical coefficients
515	$\psi_{Con.}$	Constant smoothing boundary layer
516	$\psi_{VBL\ k+1}$	Time-varying smoothing boundary layer
517	$\hat{\cdot}$	Estimated vector or values
518	\circ	Element-by-element multiplication
519	ΔH	Hydrogen higher/lower heating value (kJ/mol)
520	A	Linear system transition matrix
521	B	Input gain matrix
522	B	Parametric coefficient (V)
523	F	Faraday constant
524	H	Linear measurement matrix
525	I	Identity matrix
526	K	Kalman gain
527	P	State error covariance matrix
528	Q	Noise covariance matrix of the system
529	R	Measurement noise covariance matrix
530	k	Time index
531	n	Number of electrons transferred for each molecule of fuel
532	u	Input vector

533	v	Measurement noise vector
534	w	System noise vector
535	x	State vector
536	z	Measurement vector (system output)
537	γ	Convergence rate

538

539 **CRedit author statement**

540 **Mohsen Kandidayeni:** Conceptualization, Software, Methodology, Investigation, Writing - Original Draft. **Mehdi**
541 **Soleymani:** Writing - Review & Editing, Supervision. **Alvaro Macias:** Methodology, Software, Validation. **João P.**
542 **Trovão:** Writing - Review & Editing, Supervision, Funding acquisition. **Loïc Boulon:** Writing - Review & Editing,
543 Supervision, Funding acquisition.

544 **References**

- 545 [1] R. Arvidsson, M. Janssen, M. Svanström, P. Johansson, and B. A. Sandén, "Energy use and climate change
546 improvements of Li/S batteries based on life cycle assessment," *Journal of Power Sources*, vol. 383, pp. 87-
547 92, 2018/04/15/ 2018.
- 548 [2] O. Bamisile *et al.*, "Electrification and renewable energy nexus in developing countries; an overarching
549 analysis of hydrogen production and electric vehicles integrality in renewable energy penetration," *Energy*
550 *Conversion and Management*, vol. 236, p. 114023, 2021/05/15/ 2021.
- 551 [3] E. Pahon, D. Bouquain, D. Hissel, A. Rouet, and C. Vacquier, "Performance analysis of proton exchange
552 membrane fuel cell in automotive applications," *Journal of Power Sources*, vol. 510, p. 230385, 2021/10/31/
553 2021.
- 554 [4] S. Ahmadi, S. M. T. Bathaee, and A. H. Hosseinpour, "Improving fuel economy and performance of a fuel-
555 cell hybrid electric vehicle (fuel-cell, battery, and ultra-capacitor) using optimized energy management
556 strategy," *Energy Conversion and Management*, vol. 160, pp. 74-84, 2018/03/15/ 2018.
- 557 [5] D.-D. Tran, M. Vafaeipour, M. El Baghdadi, R. Barrero, J. Van Mierlo, and O. Hegazy, "Thorough state-of-
558 the-art analysis of electric and hybrid vehicle powertrains: Topologies and integrated energy management
559 strategies," *Renewable and Sustainable Energy Reviews*, vol. 119, p. 109596, 2020/03/01/ 2020.
- 560 [6] R. Pan, D. Yang, Y. Wang, and Z. Chen, "Health degradation assessment of proton exchange membrane fuel
561 cell based on an analytical equivalent circuit model," *Energy*, vol. 207, p. 118185, 2020/09/15/ 2020.
- 562 [7] M. Raeesi, S. Changizian, P. Ahmadi, and A. Khoshnevisan, "Performance analysis of a degraded PEM fuel
563 cell stack for hydrogen passenger vehicles based on machine learning algorithms in real driving conditions,"
564 *Energy Conversion and Management*, vol. 248, p. 114793, 2021/11/15/ 2021.
- 565 [8] K. Deng *et al.*, "Deep reinforcement learning based energy management strategy of fuel cell hybrid railway
566 vehicles considering fuel cell aging," *Energy Conversion and Management*, p. 115030, 2021/11/24/ 2021.
- 567 [9] M. Kandidayeni, A. M. Fernandez, L. Boulon, and S. Kelouwani, "Efficiency Upgrade of Hybrid Fuel Cell
568 Vehicles' Energy Management Strategies by Online Systemic Management of Fuel Cell," *IEEE Transactions*
569 *on Industrial Electronics*, pp. 1-1, 2020.
- 570 [10] H. Li, A. Ravey, A. N'Diaye, and A. Djerdir, "Online adaptive equivalent consumption minimization strategy
571 for fuel cell hybrid electric vehicle considering power sources degradation," *Energy Conversion and*
572 *Management*, vol. 192, pp. 133-149, 2019/07/15/ 2019.

- 573 [11] K. Song, Y. Ding, X. Hu, H. Xu, Y. Wang, and J. Cao, "Degradation adaptive energy management strategy
574 using fuel cell state-of-health for fuel economy improvement of hybrid electric vehicle," *Applied Energy*,
575 vol. 285, p. 116413, 2021/03/01/ 2021.
- 576 [12] D. Zhou, A. Ravey, A. Al-Durra, and F. Gao, "A comparative study of extremum seeking methods applied
577 to online energy management strategy of fuel cell hybrid electric vehicles," *Energy Conversion and*
578 *Management*, vol. 151, pp. 778-790, 2017/11/01/ 2017.
- 579 [13] D. Zhou, A. Al-Durra, I. Matraji, A. Ravey, and F. Gao, "Online Energy Management Strategy of Fuel Cell
580 Hybrid Electric Vehicles: A Fractional-Order Extremum Seeking Method," *IEEE Transactions on Industrial*
581 *Electronics*, vol. 65, no. 8, pp. 6787-6799, 2018.
- 582 [14] Q. Li *et al.*, "Online extremum seeking-based optimized energy management strategy for hybrid electric tram
583 considering fuel cell degradation," *Applied Energy*, Article vol. 285, 2021, Art. no. 116505.
- 584 [15] T. Wang *et al.*, "An optimized energy management strategy for fuel cell hybrid power system based on
585 maximum efficiency range identification," *Journal of Power Sources*, Article vol. 445, 2020, Art. no. 227333.
- 586 [16] T. Wang, Q. Li, Y. Qiu, L. Yin, L. Liu, and W. Chen, "Efficiency Extreme Point Tracking Strategy Based
587 on FFRLS Online Identification for PEMFC System," *IEEE Transactions on Energy Conversion*, vol. 34,
588 no. 2, pp. 952-963, 2019.
- 589 [17] T. Wang, Q. Li, L. Yin, and W. Chen, "Hydrogen consumption minimization method based on the online
590 identification for multi-stack PEMFCs system," *International Journal of Hydrogen Energy*, vol. 44, no. 11,
591 pp. 5074-5081, 2019/02/26/ 2019.
- 592 [18] Q. Li *et al.*, "Online extremum seeking-based optimized energy management strategy for hybrid electric tram
593 considering fuel cell degradation," *Applied Energy*, vol. 285, p. 116505, 2021/03/01/ 2021.
- 594 [19] K. Ettihir, L. Boulon, M. Becherif, K. Agbossou, and H. S. Ramadan, "Online identification of semi-
595 empirical model parameters for PEMFCs," *International Journal of Hydrogen Energy*, Article vol. 39, no.
596 36, pp. 21165-21176, 2014.
- 597 [20] G. Squadrito, G. Maggio, E. Passalacqua, F. Lufrano, and A. Patti, "An empirical equation for polymer
598 electrolyte fuel cell (PEFC) behaviour," *Journal of Applied Electrochemistry*, vol. 29, no. 12, pp. 1449-1455,
599 1999/12/01 1999.
- 600 [21] K. Ettihir, M. Higueta Cano, L. Boulon, and K. Agbossou, "Design of an adaptive EMS for fuel cell vehicles,"
601 *International Journal of Hydrogen Energy*, Article vol. 42, no. 2, pp. 1481-1489, 2017.
- 602 [22] M. Kandidayeni, A. Macias, A. A. Amamou, L. Boulon, S. Kelouwani, and H. Chaoui, "Overview and
603 benchmark analysis of fuel cell parameters estimation for energy management purposes," *Journal of Power*
604 *Sources*, Article vol. 380, pp. 92-104, 2018.
- 605 [23] J. C. Amphlett, "Performance Modeling of the Ballard Mark IV Solid Polymer Electrolyte Fuel Cell," *Journal*
606 *of The Electrochemical Society*, vol. 142, no. 1, p. 9, 1995.
- 607 [24] R. F. Mann, J. C. Amphlett, M. A. I. Hooper, H. M. Jensen, B. A. Peppley, and P. R. Roberge, "Development
608 and application of a generalised steady-state electrochemical model for a PEM fuel cell," *Journal of Power*
609 *Sources*, vol. 86, no. 1, pp. 173-180, 2000/03/01/ 2000.
- 610 [25] A. Amamou, M. Kandidayeni, A. Macias, L. Boulon, and S. Kelouwani, "Efficient model selection for real-
611 time adaptive cold start strategy of a fuel cell system on vehicular applications," *International Journal of*
612 *Hydrogen Energy*, vol. 45, no. 38, pp. 19664-19675, 2020/07/31/ 2020.
- 613 [26] M. Kandidayeni, A. Macias, A. Khalatbarisoltani, L. Boulon, and S. Kelouwani, "Benchmark of proton
614 exchange membrane fuel cell parameters extraction with metaheuristic optimization algorithms," *Energy*,
615 vol. 183, pp. 912-925, 2019/09/15/ 2019.
- 616 [27] S. Xu, Y. Wang, and Z. Wang, "Parameter estimation of proton exchange membrane fuel cells using eagle
617 strategy based on JAYA algorithm and Nelder-Mead simplex method," *Energy*, vol. 173, pp. 457-467,
618 2019/04/15/ 2019.
- 619 [28] E. A. Gouda, M. F. Kotb, and A. A. El-Fergany, "Jellyfish search algorithm for extracting unknown
620 parameters of PEM fuel cell models: Steady-state performance and analysis," *Energy*, vol. 221, p. 119836,
621 2021/04/15/ 2021.
- 622 [29] M. Kandidayeni, A. Macias, A. A. Amamou, L. Boulon, and S. Kelouwani, "Comparative Analysis of Two
623 Online Identification Algorithms in a Fuel Cell System," *Fuel Cells*, Article vol. 18, no. 3, pp. 347-358, 2018.
- 624 [30] A. Daeichian, R. Ghaderi, M. Kandidayeni, M. Soleymani, J. P. Trovão, and L. Boulon, "Online
625 characteristics estimation of a fuel cell stack through covariance intersection data fusion," *Applied Energy*,
626 vol. 292, p. 116907, 2021/06/15/ 2021.
- 627 [31] Y. Xing, J. Na, and R. Costa-Castelló, "Real-Time Adaptive Parameter Estimation for a Polymer Electrolyte
628 Membrane Fuel Cell," *IEEE Transactions on Industrial Informatics*, vol. 15, no. 11, pp. 6048-6057, 2019.

- 629 [32] M. Kandidayeni, H. Chaoui, L. Boulon, S. Kelouwani, and J. P. F. Trovao, "Online System Identification of
630 a Fuel Cell Stack with Guaranteed Stability for Energy Management Applications," *IEEE Transactions on*
631 *Energy Conversion*, pp. 1-1, 2021.
- 632 [33] H. Chaoui, M. Kandidayeni, L. Boulon, S. Kelouwani, and H. Gualous, "Real-Time Parameter Estimation of
633 a Fuel Cell for Remaining Useful Life Assessment," *IEEE Transactions on Power Electronics*, vol. 36, no.
634 7, pp. 7470-7479, 2021.
- 635 [34] S. Habibi, "The Smooth Variable Structure Filter," *Proceedings of the IEEE*, vol. 95, no. 5, pp. 1026-1059,
636 2007.
- 637 [35] M. Avzayesh, M. Abdel-Hafez, M. AlShabi, and S. A. Gadsden, "The smooth variable structure filter: A
638 comprehensive review," *Digital Signal Processing*, vol. 110, p. 102912, 2021/03/01/ 2021.
- 639 [36] T. Kim, Y. Wang, Z. Sahinoglu, T. Wada, S. Hara, and W. Qiao, "State of charge estimation based on a
640 realtime battery model and iterative smooth variable structure filter," in *2014 IEEE Innovative Smart Grid*
641 *Technologies - Asia (ISGT ASIA)*, 2014, pp. 132-137.
- 642 [37] H. H. Afshari, M. Attari, R. Ahmed, A. Delbari, S. Habibi, and T. Shoa, "Reliable state of charge and state
643 of health estimation using the smooth variable structure filter," *Control Engineering Practice*, vol. 77, pp. 1-
644 14, 2018/08/01/ 2018.
- 645 [38] S. A. Gadsden and S. R. Habibi, "A New Robust Filtering Strategy for Linear Systems," *Journal of Dynamic*
646 *Systems, Measurement, and Control*, vol. 135, no. 1, 2012.
- 647 [39] S. A. Gadsden, M. Al-Shabi, I. Arasaratnam, and S. R. Habibi, "Combined cubature Kalman and smooth
648 variable structure filtering: A robust nonlinear estimation strategy," *Signal Processing*, vol. 96, pp. 290-299,
649 2014/03/01/ 2014.
- 650 [40] W. Youn and S. A. Gadsden, "Combined Quaternion-Based Error State Kalman Filtering and Smooth
651 Variable Structure Filtering for Robust Attitude Estimation," *IEEE Access*, vol. 7, pp. 148989-149004, 2019.
- 652 [41] F. Demim, S. Benmansour, N. Abdelkrim, A. Rouigueb, M. Hamerlain, and A. Bazoula, "Simultaneous
653 localisation and mapping for autonomous underwater vehicle using a combined smooth variable structure
654 filter and extended kalman filter," *Journal of Experimental & Theoretical Artificial Intelligence*, pp. 1-30,
655 2021.
- 656 [42] R. O'Hayre, S.-W. Cha, W. Colella, and F. B. Prinz, "Chapter 1: Introduction," in *Fuel Cell Fundamentals*,
657 2016, pp. 1-24.
- 658 [43] J. Larminie and A. Dicks, "Operational Fuel Cell Voltages," in *Fuel Cell Systems Explained*, 2003, pp. 45-
659 66.
- 660 [44] A. Saadi, M. Becherif, A. Aboubou, and M. Y. Ayad, "Comparison of proton exchange membrane fuel cell
661 static models," *Renewable Energy*, vol. 56, pp. 64-71, 2013/08/01/ 2013.
- 662 [45] F. Barbir, "CHAPTER 3 - Fuel Cell Electrochemistry," in *PEM Fuel Cells*, F. Barbir, Ed. Burlington:
663 Academic Press, 2005, pp. 33-72.
- 664 [46] S. Haykin, "Kalman Filters," in *Kalman Filtering and Neural Networks*, 2001, pp. 1-21.
- 665 [47] S. A. Gadsden, S. Habibi, and T. Kirubarajan, "Kalman and smooth variable structure filters for robust
666 estimation," *IEEE Transactions on Aerospace and Electronic Systems*, vol. 50, no. 2, pp. 1038-1050, 2014.
- 667 [48] K. Ettihir, L. Boulon, and K. Agbossou, "Optimization-based energy management strategy for a fuel
668 cell/battery hybrid power system," *Applied Energy*, Article vol. 163, pp. 142-153, 2016.
- 669 [49] M. Kandidayeni, A. O. Macias Fernandez, A. Khalatbarisoltani, L. Boulon, S. Kelouwani, and H. Chaoui,
670 "An Online Energy Management Strategy for a Fuel Cell/Battery Vehicle Considering the Driving Pattern
671 and Performance Drift Impacts," *IEEE Transactions on Vehicular Technology*, Article vol. 68, no. 12, pp.
672 11427-11438, 2019, Art. no. 8809281.

673